CrossMark

RESEARCH PAPER

Structured model and parameter estimation in plant cell cultures of *Thevetia peruviana*

Adriana Villegas[1,3] · Juan Pablo Arias[2] · Daira Aragón[4] · Silvia Ochoa[1] ·
Mario Arias[2]

Abstract In this work, a mechanistic model for predicting the dynamic behavior of extracellular and intracellular nutrients, biomass production, and the main metabolites involved in the central carbon metabolism in plant cell cultures of *Thevetia peruviana* is presented. The proposed model is the first mechanistic model implemented for plant cell cultures of this species, and includes 28 metabolites, 33 metabolic reactions, and 61 parameters. Given the over-parametrization of the model, its nonlinear nature and the strong correlation among the effects of the parameters, a parameter estimation routine based on identifiability analysis was implemented. This routine reduces the parameter's search space by selecting the most sensitive and linearly independent parameters. Results have shown that only 19 parameters are identifiable. Finally, the model was used for analyzing the fluxes distribution in plant cell cultures of *T. peruviana*. This analysis shows high uptake of phosphates and parallel uptake of glucose and fructose. Furthermore, it has pointed out the main central carbon
metabolism routes for promoting biomass production in this cell culture.

Keywords *Thevetia peruviana* · Plant cell cultures · Modelling · Parameter estimation · Identifiability analysis

Introduction

Thevetia peruviana is a very promising plant for in vitro cultures, because it produces several compounds with applications in pharmaceutical industries [1, 2]. Among the compounds produced from this culture, the cardiac glycosides are particularly important given their applications in the treatment of cardiac diseases. Several studies have obtained cardiac glycosides from this plant. Kohls et al. [3] and Tian et al. [4] isolated several types of cardiac glycosides from seeds of *T. peruviana*. On the other hand, Arias et al. [1] and Amaringo et al. [5] have reported the production of Peruvoside and Thevetin B, respectively, in plant cell suspensions of this species. Despite of the important metabolites that can be produced from *T. peruviana,* only very few works reported in the open literature have addressed the in vitro production of these plant cells [1, 2, 5, 6]. Furthermore, to the authors' knowledge, this work is the first one developing a mechanistic model to describe the cell growth, nutrients uptake, and dynamic behavior of the main metabolites on the central carbon metabolism in plant cell cultures of *T. peruviana*. The strategy followed for obtaining the model includes the following steps: (a) gathering of experimental data (b) proposal of the kinetic model, (c) parameter estimation, and (d) model validation. In the first step, cultivation of cells was performed under batch operation in shake flask to determine dynamics of cell growth, extracellular sugars

✉ Adriana Villegas
adriana.villegas@ucc.edu.co

1 Research Group on Simulation, Design, Control and Optimization of Chemical Processes (SIDCOP), Faculty of Engineering, Universidad de Antioquia, Calle 67 No 53, 108, Medellín, Colombia

2 Research Group in Industrial Biotechnology, Faculty of Sciences, Universidad Nacional de Colombia Sede Medellín, Calle 59ª, No 63-20, Medellín, Colombia

3 Termomec Research Group, Faculty of Engineering, Universidad Cooperativa de Colombia. Calle 48 No 28-00, Medellín, Colombia

4 Audubon Sugar Institute, LSU AgCenter. United States. 3845 Highway 75, St Gabriel, LA, 70776 USA

and nitrates uptake, and intracellular sugars, nitrates, and phosphates uptake. Second, a mechanistic model for plant cell cultures of *T. peruviana*, based on the previous works by Cloutier et al. [7] and Leduc et al. [8], is proposed. This model is divided in three compartments: extracellular, intracellular, and central primary metabolism. The model considers the reactions for cell growth and includes a term to describe the initial accumulation of extracellular nitrates in this species. The proposed model includes 28 metabolic species and comprises 33 metabolic reactions, and 61 parameters. Given the issues associated with the over-parametrization of the model, its nonlinear nature and the strong correlation among the effects of the parameters, the parameter estimation routine includes a step of identifiability analysis. In practical identifiability analysis, a subset of parameters for estimation (Subset Selection) is determined considering the influence of the selected parameters on the model and the correlations among the effects of the parameters. Therefore, an ill posed problem is transformed into a well-posed one [9–18]. In this work, the algorithm for subset selection proposed by Yao et al. [18] to determine the most sensitive and linearly independent parameters is implemented. The proposed model is validated using a new set of experimental data and calculating the confidence intervals for the subset of identifiable parameters. Finally, the validated model is used to determine the distribution of fluxes in plant cell cultures of *T. peruviana*.

Model development

Many biological processes, such as metabolism of a cell culture and cellular stress responses, are nonstationary in their nature [19]. Therefore, dynamic models are preferred to describe the changes in the main state variables for these processes. In general terms, two types of dynamic structured models can be differentiated in the literature, simple structured models and mechanistic models. In the case of plant cell cultures, some simple structured models have been reported by Bramble et al. [20], Hooker and Lee [21], Van Gulik et al. [22], Takeda et al. [23], Choi et al. [24, 25], Schlatmann et al. [26], Pires Cabral et al. [27], Zhang and Su [28], Li et al. [29], and Cloutier et al. [7]. These models are organized in pools that include general information about the activity and functions of the nutrients inside the cells. However, they do not use information about the kinetic reactions for biomass growth and metabolite production, since the cellular reactions are normally empirical and they do not represent the true conversion between components [30, 31]. Mechanistic models give a good representation of the intracellular processes by including balances of intracellular compounds and stoichiometric steps [30]. The metabolic networks are

described by ordinary differential equations that represent mass balances of the substrate, biomass, products, and intracellular metabolites, as well as numerous reactions rates corresponding to the pathways [32, 33]. With the solution of this dynamic system, it is possible to obtain information about concentration profiles of each species and flux distribution over time. This information can be useful to evaluate the changes needed to optimize the production of biomass and metabolites of interest based on quantities, such as the flux of different compounds.

Some mechanistic models have been proposed in the literature for plant cell cultures and hairy roots. Leduc et al. [8] presents a model to describe the cell growth and intracellular transport and accumulation of nutrients in *Catharanthus roseus* hairy roots. The metabolic network includes glycolysis, pentose-phosphate pathway, TCA cycle, energy shuttles, and cofactors. The secondary metabolism is included in the model considering the metabolisms derived from tryptamine and secologanin. The metabolic network is divided into two interlinked subnet-works as the stationary primary metabolism (including glycolysis, TCA cycle, and cell building blocks, such as amino acids, lipids, and organic acids among others) and transient metabolism (including cell growth nutrient transport between medium and intracellular volumes). Cloutier et al. [34] present a dynamic model for the primary metabolism of plant cells and hairy roots based on the modelling approach presented in Leduc et al. [8] but without the steady-state assumption on the primary metabolism. Sigmoid switch functions are multiplied by the reaction rates to reduce discontinuities around the threshold values. Cloutier et al. [35] used the model proposed by Cloutier et al. [34] for the identification and control of intracellular phosphate dynamics in plant cell cultures of *Eschscholtiza californica*. Cloutier et al. [36] used the model of Cloutier et al. [35] for developing the optimization of the production of alkaloid production from cell cultures of *Eschscholtiza californica*.

The mechanistic model proposed in this work for plant cell cultures of *T. peruviana* is based on the works by Cloutier et al. [34] and Leduc et al. [8]. The model is described by the first principles-based model derived from the mass balances, as follows:

$$\frac{\mathrm{d}X}{\mathrm{d}t} = f(X, t, \theta) \quad X(t_0) = X_0 \tag{1}$$

$$Y = g(X, t, \theta) \tag{2}$$

where $X = [x_1, x_2, \ldots, x_r]$ indicates the state variable vector, t is the time, $\theta = [\theta_1, \theta_2, \ldots, \theta_m]$ is the vector of model parameters, X_0 is the vector of initial conditions, and $Y = [y_1, y_2, \ldots, y_n]$ correspond to the model output vector, with $n \leq r$. The nomenclature used for the state and output

variables is presented in Tables 1 and 2, respectively. The initial conditions for the state variables were taken from literature [7, 8, 34, 37] and their values are reported in Table 1.

Figure 1 shows the pathway for biomass production, while the reactions considered at each step are presented in Table 3. For this culture, only the reactions of the central carbon metabolism for biomass production were considered. Other considerations considered when formulating the model include

- Different to case of Leduc et al. [8], and following the proposal of Cloutier et al. [34], this model does not consider the steady-state hypothesis on the primary metabolism.
- The extracellular compartment is formed by the main nutrients for cell growth in plant cells: ESUC, ENO_3, and EPi. The ESUC is hydrolyzed into EGLUC and EFRUC in reaction (1). According to the experimental results, this hydrolysis is carried out mainly at extracellular level, different to the case reported by Cloutier et al. [35] in which the analysis of the intracellular hydrolysis of sucrose into glucose and fructose for cell cultures of *Eschscholtiza californica* was included. The extracellular hydrolysis of sucrose into glucose and fructose in plant cell cultures can be due to the presence of the invertase enzyme [38]. Such extracellular hydrolysis has been reported by Choi et al. [39] for cell suspensions of *Glycyrrhiza inflate*, Shibasaki et al.

Table 2 Output variables **Y**

| Symbol	Name	Units
x	Biomass	g/L
ESUC	Extracellular sucrose	mM
EGLUC	Extracellular glucose	mM
EFRUC	Extracellular fructose	mM
GLUC	Intracellular glucose	mmolg DW^{-1}
ENO_3	Extracellular nitrates	mM
NO_3	Intracellular nitrates	mmolg DW^{-1}
Pi	Intracellular phosphate	mmolg DW^{-1}

[24] for cell suspensions of *Thalictrum rugosum*, Westgate et al. [40] for cell suspensions of *Nicotiana tabacum*, and Li et al. [41] for cell suspensions of *Cephalotaxus harringtonia*.

- In the intracellular compartment, all fructose has turned into glucose, according to reaction (3). All NO_3 is formed from ENO_3 in reaction (17), and then it is transformed into NH_4 in reaction (18). The total Pi is obtained from EPi in reaction (20) and from all intermediate reactions of the central metabolism involving the formation and consumption of this species.
- Central primary metabolism compartment details the reactions of the precursors for the biomass formation. STH,OP,LIP,ORA, and AA are considered the biomass precursors according to reaction (31) [7, 8]. The STH

Table 1 State variables **X**

Symbol	Name	Initial Conditions	Units
G6P	Glucose-6-phosphate	0.0122	mmolg DW^{-1}
R5P	Ribulose-6-phosphate	1.26×10^{-4}	mmolg DW^{-1}
F6P	Fructose-6-phosphate	0.0012	mmolg DW^{-1}
G3P	Glyceraldehido-3-phosphate	0.5000	mmolg DW^{-1}
PEP	Phosphoenolpyruvate	7.25×10^{-6}	mmolg DW^{-1}
PYR	Pyruvate	1.30×10^{-6}	mmolg DW^{-1}
ACOA	Acetyl-Co-A	1.24×10^{-6}	mmolg DW^{-1}
OXO	Oxoglutarate	1.21×10^{-6}	mmolg DW^{-1}
OAA	Oxaloacetate	1.26×10^{-6}	mmolg DW^{-1}
NH_4	Ammonium	0.0530	mmolg DW^{-1}
O_2	Oxygen	700.3000	mmolg DW^{-1}
STA	Starch	0.00505	mmolg DW^{-1}
STH	Structural hexoses	0.001	mmolg DW^{-1}
OP	Organic phosphates	6.5×10^{-4}	mmolg DW^{-1}
LIP	Lipids	0.1000	mmolg DW^{-1}
ORA	Organic acids	0.0807	mmolg DW^{-1}
AA	Amino acids	0.1260	mmolg DW^{-1}
CO_2	Carbon dioxide	30.5000	mmolg DW^{-1}
EPi	Extracellular phosphate	4.1200	mM
PPi	Pyrophosphate	0.00035	mmolg DW^{-1}
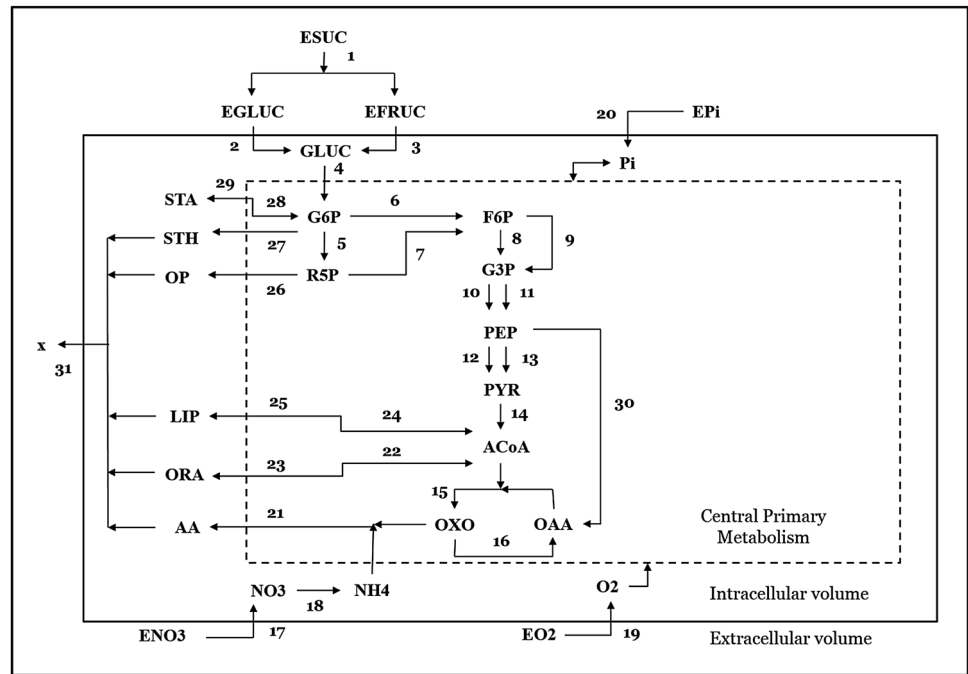
and OP are formed through the species GLUC, G6P in reactions (4) and (27), and GLUC, G6P, and R5P in reactions (4), (5), and (26), respectively. The LIP and ORA are formed from reversible reactions from ACOA. The ACOA is formed from the PYR, in reaction (14), which is obtained from glycolysis pathway, in reactions (4), (6), (8), (9), (10), (11), (12), and (13). Finally, the AA are formed from fixation of NH_4, and OXO which is formed from TCA cycle, reactions (15) and (16), including the reaction (30), in which the OAA is formed from PEP. In this model, the intracellular STA is considered as a storage carbon source [42]. The AA is only used to form biomass (the endogenous behavior is not considered in the model). Finally, the energy shuttles ADP and ATP, cofactors NADH and NSDPH, and their oxidized forms NAD and NADP are considered in steady state.

Each pathway regulation (reaction rate) is described by multiplicative Michaelis–Menten equation as shown in Eq. (3), indicating the effect of the substrates involved, where each flux has a maximum reaction rate $v_{max(j)}$ and an affinity constant K_{m_i}. The expressions for the fluxes are presented in Table 4. Reaction rate $v(17)$ presents an additional inhibition term expression with a constant of inhibition $KIENO_3$ to include the effect of accumulation of extracellular nitrates. The reaction rates for extracellular nitrates and phosphates use simple Michaelis–Menten expressions, different to the reactions rates presented by Cloutier et al. [34] that include double Michaelis–Menten-type expressions. The reaction rates in this work are not

multiplied by sigmoid switch functions, since the discontinuities around the threshold are evaluated by the use of sensitivity matrix. Therefore, the kinetic expressions are significantly different to the previous works by Leduc et al. [8] and Cloutier et al. [34]:

$$v(j) = v_{\max(j)} \prod_i \frac{x_i}{K_{m_i} + x_i}. \tag{3}$$

The dynamic model proposed consists of the mass balance equations for extracellular and intracellular nutrients, as presented in the following equation:

$$\frac{dX}{dt} = \sum_j r_{ij} v_j - \mu x_i \tag{4}$$

where μ is the specific growth rate presented in Eq. (5) and r_{ij} is the stoichiometric coefficient for each metabolite in the reaction j

$$\mu = v_{\max(31)} \times \frac{AA}{K_m AA + AA} \times \frac{STH}{K_m STH + STH}$$
$$\times \frac{LIP}{K_m LIP + LIP} \times \frac{ORA}{K_m ORA + ORA} \times \frac{OP}{K_m OP + OP}. \tag{5}$$

Parameter estimation and model validation

The objective function used for solving the parameter estimation problem is expressed as the sum of squared errors (MSE_Y) [Eq. (6)]

$$\min J(\boldsymbol{\theta}) = \sum_{i=1}^{n} MSE_Y. \tag{6}$$

Table 3 Reactions of metabolic network considered in the model proposed for plant cell cultures of *Thevetia peruviana*

No.	Reactions	References
1	ESUC → EGLUC + EFRUC	[34]
2	EGLUC + ATP → GLUC + ADP + Pi	[34, 43]
3	EFRUC + ATP → FRUC + ADP + Pi	[34, 43]
	FRUC → GLUC	[8]
4	GLUC + ATP → G6P + ADP	[34]
5	G6P + 2NADP → R5P + 2NADPH	[34]
6	G6P → F6P	[34]
7	R5P → 2F6P + G3P	[34]
8	F6P + ATP → 2G3P + ADP	[34]
9	F6P + PPi → 2G3P + Pi	[34]
10	G3P + Pi + ADP + NAD → PEP + ATP + NADH	[34]
11	G3P + NADP → PEP + NADPH	[34]
12	PEP → PYR + Pi	[34]
13	PEP + ADP → PYR + ATP	[34]
14	PYR + NAD → NADH + ACOA	[34]
15	ACOA + OAA + NAD → OXO + NADH	[34]
16	OXO + 2NAD + ADP + Pi → OAA + 2NADH + ATP	[34]
17	ENO$_3$ + ATP → NO$_3$ + ADP + Pi	[34]
18	NO$_3$ + NADH + 3NADPH → NH$_4$ + NAD + 3NADP	[34]
19	2.5ADP + 2.5Pi + NADH + O$_2$ → 2.5ATP + NAD	[34]
20	EPi + 2ATP → 3Pi + 2ADP	[34]
21	OXO + NH$_4$ + 3NADPH + 3ATP → AA + 3NADP + 3ADP + 3Pi	[34]
22	ORA → ACOA	[34]
23	ACOA → ORA	[34]
24	LIP + 2ATP + NAD → ACOA + 2ADP + PPi + NADH	[34]
25	ACOA + ATP + 2NADPH → LIP + ADP + Pi + 2NADP	[34]
26	R5P + 3.75AA + ATP + 0.25NAD → 7ADP + 3.5Pi + 1.75PPi + 0.25NADH + OP	[34]
27	G6P + 2ATP + NADPH → STH + 2ADP + NADP + Pi + PPi	[34]
28	STA + Pi → G6P	[34, 42]
29	G6P + ATP → STA + ADP + PPi	[34, 42]
30	PEP + CO$_2$ → OAA + Pi	[34]
31	AA + LIP + ORA + STH + OP → x	[34]
32	PPi → 2Pi	[34]
33	OP → Pi	[34]

The MSE$_Y$ for each variable is defined by the following equation:

$$\mathrm{MSE_Y} = \frac{1}{n} \sum_{i=1}^{n} \left(Y_{\mathrm{exp},i} - Y_i \right)^2 \tag{7}$$

where $Y_{exp,i}$ corresponds to the experimental points. The initial parameter values θ_0 to solve the optimization problem were taken from other similar works in plant cell cultures [7, 35, 37]. Two sets of experimental data were used for parameter identification, whereas one different data set was used for model validation. Each experimental data set was obtained at different initial sucrose and inoculum concentrations. Simulated Annealing optimization algorithm was used for solving the parameter estimation problem until obtaining an initial pseudo-optimal set of parameter values θ^*. This set of parameters is presented in Table 5.

To solve the issues associated with the over-parametrization of the model, its nonlinear nature, and the strong correlation among the effects of the parameters, identifiability analysis was carried out for establishing a new subset of identifiable parameters $\theta_k \subset \theta^*$ that presents a high effect in the objective function, and low linear dependency. The remaining parameters (i.e., those non-identifiable) are fixed at their initial values, forming the subset $\theta_{\mathbf{Fixed}}$. A new optimization routine is performed

Table 4 Kinetic equations proposed in the case of plant cell cultures of *Thevetia peruviana*

No.	Kinetic equations
1	$v(1) = v_{max(1)} \times \text{ESUC}/(\text{KmESUC} + \text{ESUC})$
2	$v(2) = v_{max(2)} \times \text{EGLUC}/(\text{KmEGLUC} + \text{EGLUC})$
3	$v(3) = v_{max(3)} \times \text{EFRUC}/(\text{KmEFRUC} + \text{EFRUC})$
4	$v(4) = v_{max(4)} \times \text{GLUC}/(\text{KmGLUC} + \text{EGLUC})$
5	$v(5) = v_{max(5)} \times \text{G6P}/(\text{KmG6P} + \text{G6P})$
6	$v(6) = v_{max(6)} \times \text{G6P}/(\text{KmG6P} + \text{G6P})$
7	$v(7) = v_{max(7)} \times \text{R5P}/(\text{KmR5P} + \text{R5P})$
8	$v(8) = v_{max(8)} \times \text{F6P}/(\text{KmF6P} + \text{F6P})$
9	$v(9) = v_{max(9)} \times \dfrac{\text{F6P}}{\text{KmF6P} + \text{F6P}} \times \dfrac{\text{PPi}}{\text{KmPPi} + \text{PPi}}$
10	$v(10) = v_{max(10)} \times \dfrac{\text{G3P}}{\text{KmG3P} + \text{G3P}} \times \dfrac{\text{Pi}}{\text{KmPi} + \text{Pi}}$
11	$v(11) = v_{max(11)} \times \text{G3P}/(\text{KmG3P} + \text{G3P})$
12	$v(12) = v_{max(12)} \times \text{PEP}/(\text{KmPEP} + \text{PEP})$
13	$v(13) = v_{max(13)} \times \text{PEP}/(\text{KmPEP} + \text{PEP})$
14	$v(14) = v_{max(14)} \times \text{PYR}/(\text{KmPYR} + \text{PYR})$
15	$v(15) = v_{max(15)} \times \dfrac{\text{ACOA}}{\text{KmACOA} + \text{ACOA}} \times \dfrac{\text{OAA}}{\text{KmOAA} + \text{OAA}}$
16	$v(16) = v_{max(16)} \times \dfrac{\text{OXO}}{\text{KmOXO} + \text{OXO}} \times \dfrac{\text{Pi}}{\text{KmPi} + \text{pI}}$
17	$v(17) = v_{max(17)} \times \dfrac{\text{ENO}_3}{\text{KmENO}_3 + \text{ENO}_3} \times \dfrac{\text{KIENO}_3}{\text{KIENO}_3 + \text{ENO}_3}$
18	$v(18) = v_{max(18)} \times \text{NO}_3/(\text{KmNO}_3 + \text{NO}_3)$
19	$v(19) = v_{max(19)} \times \dfrac{\text{Pi}}{\text{KmPi} + \text{Pi}} \times \dfrac{\text{O}_2}{\text{KmO}_2 + \text{O}_2}$
20	$v(20) = v_{max(20)} \times \text{EPi}/(\text{KmEPi} + \text{EPi})$
21	$v(21) = v_{max(21)} \times \dfrac{\text{OXO}}{\text{KmOXO} + \text{OXO}} \times \dfrac{\text{NH}_4}{\text{KmNH}_4 + \text{NH}_4}$
22	$v(22) = v_{max(22)} \times \text{ORA}/(\text{KmORA} + \text{ORA})$
23	$v(23) = v_{max(23)} \times \text{ACOA}/(\text{KmACOA} + \text{ACOA})$
24	$v(24) = v_{max(24)} \times \text{LIP}/(\text{KmLIP} + \text{LIP})$
25	$v(25) = v_{max(25)} \times \text{ACOA}/(\text{KmACOA} + \text{ACOA})$
26	$v(26) = v_{max(26)} \times \dfrac{\text{R5P}}{\text{KmR5P} + \text{R5P}} \times \dfrac{\text{AA}}{\text{KmAA} + \text{AA}}$
27	$v(27) = v_{max(27)} \times \text{G6P}/(\text{KmG6P} + \text{G6P})$
28	$v(28) = v_{max(28)} \times \text{STA}/(\text{KmSTA} + \text{STA})$
29	$v(29) = v_{max(29)} \times \text{G6P}/(\text{KmG6P} + \text{G6P})$
30	$v(30) = v_{max(30)} \times \dfrac{\text{PEP}}{\text{KmPEP} + \text{PEP}} \times \dfrac{\text{CO}_2}{\text{KmCO}_2 + \text{CO}_2}$
31	$v(31) = v_{max(31)} \times \dfrac{\text{AA}}{\text{KmAA} + \text{AA}} \times \dfrac{\text{STH}}{\text{KmSTH} + \text{STH}} \times \dfrac{\text{LIP}}{\text{KmLIP} + \text{LIP}} \times \dfrac{\text{ORA}}{\text{KmORA} + \text{ORA}} \times \dfrac{\text{OP}}{\text{KmOP} + \text{OP}} \times x$
32	$v(32) = v_{max(32)} \times \text{PPi}/(\text{KmOP} + \text{PPi})$
33	$v(31) = v_{max(33)} \times \text{OP}/(\text{KmOP} + \text{OP})$

where the decision variables are the parameters in the subset θ_k, until a new optimal subset of parameters θ_k^* is obtained. The new set of optimal parameters is $\left\{ \tilde{\theta} = \theta_k^* \cup \theta_{\text{Fixed}} \right\}$. If this set of parameters presents a good fit, it will be taken as the final set of optimal parameters, in the opposite case, it will be necessary to restart the estimation process taking $\theta_0 = \tilde{\theta}$.

To determine the subset of identifiable parameters, a local sensitivity analysis was performed based on the sensitivity matrix. This matrix denotes the relationship between the derivatives of the state variables of the model

x_i with respect to the parameters θ_j as it is presented in the following equation [44]:

$$Z = \frac{\partial X}{\partial \theta} = \begin{bmatrix} \dfrac{\partial x_1}{\partial \theta_1} & \dfrac{\partial x_1}{\partial \theta_2} & \cdots & \dfrac{\partial x_1}{\partial \theta_m} \\ \dfrac{\partial x_2}{\partial \theta_1} & \dfrac{\partial x_2}{\partial \theta_2} & \cdots & \dfrac{\partial x_2}{\partial \theta_m} \\ \vdots & \vdots & & \vdots \\ \dfrac{\partial x_n}{\partial \theta_1} & \dfrac{\partial x_n}{\partial \theta_2} & \cdots & \dfrac{\partial x_n}{\partial \theta_m} \end{bmatrix}. \tag{8}$$

Sensitivity functions were derived by integrating the original model along with the sensitivity equations

Table 5 Initial and pseudo-optimal parameter values for affinity constants K_M and maximum reaction rates v_{max} in the proposed model

Parameter number	Symbols	Units	Initial parameters value θ_0	Pseudo-optimal initial set θ^*
1	KmESUC	mM	36.4400	24.8394
2	KmEGLUC	mM	73.4100	34.7882
3	KmEFRUC	mM	46.9200	76.2353
4	KmGLUC	mmolg DW^{-1}	0.8454	0.3625
5	KmG6P	mmolg DW^{-1}	0.7708	0.6912
6	KmR5P	mmolg DW^{-1}	0.9130	0.3631
7	KmF6P	mmolg DW^{-1}	0.6094	0.2498
8	KmG3P	mmolg DW^{-1}	0.4495	0.4845
9	KmPEP	mmolg DW^{-1}	0.9806	0.7138
10	KmPYR	mmolg DW^{-1}	0.9995	0.3911
11	KmACOA	mmolg DW^{-1}	0.2992	0.3968
12	KmOXO	mmolg DW^{-1}	0.6259	0.8660
13	KmOAA	mmolg DW^{-1}	0.3103	0.6911
14	KmENO$_3$	mM	31.0300	37.7649
15	KmNO$_3$	mmolg DW^{-1}	0.2644	0.8806
16	KmNH$_4$	mmolg DW^{-1}	0.2971	0.6995
17	KmO$_2$	mmolg DW^{-1}	3.97×10^{-8}	4×10^{-8}
18	KmEPi	mM	3.2000	16.6949
19	KmPi	mmolg DW^{-1}	0.0385	0.7573
20	KmSTA	mmolg DW^{-1}	0.0290	0.0538
21	KmOP	mmolg DW^{-1}	0.3393	0.2321
22	KmLIP	mmolg DW^{-1}	0.7445	0.7066
23	KmORA	mmolg DW^{-1}	0.0089	0.0575
24	KmAA	mmolg DW^{-1}	0.0574	0.0871
25	KmCO$_2$	mmolg DW^{-1}	0.0083	0.0017
26	KmPPi	mmolg DW^{-1}	0.0043	0.0054
27	KmSTH	mmolg DW^{-1}	0.0142	0.0798
59	KIENO$_3$	mmolg DW^{-1}	5.1140	8.2748
28	$v_{\max}(1)$	mmolg DW^{-1} day^{-1}	14.2400	15.1748
29	$v_{\max}(2)$	mmolg DW^{-1} day^{-1}	55.1700	44.0409
30	$v_{\max}(3)$	mmolg DW^{-1} day^{-1}	38.0900	67.8724
31	$v_{\max}(4)$	mmolg DW^{-1} day^{-1}	162.3800	63.6234
32	$v_{\max}(5)$	mmolg DW^{-1} day^{-1}	8.3611	8.8845
33	$v_{\max}(6)$	mmolg DW^{-1} day^{-1}	2.1774	6.3287
34	$v_{\max}(7)$	mmolg DW^{-1} day^{-1}	3.7152	3.0724
35	$v_{\max}(8)$	mmolg DW^{-1} day^{-1}	8.1320	3.3733
36	$v_{\max}(9)$	mmolg DW^{-1} day^{-1}	0.0087	0.0026
37	$v_{\max}(10)$	mmolg DW^{-1} day^{-1}	46.3235	54.6006
38	$v_{\max}(11)$	mmolg DW^{-1} day^{-1}	1.39×10^{-5}	1.04×10^{-5}
39	$v_{\max}(12)$	mmolg DW^{-1} day^{-1}	0.0036	0.0089
40	$v_{\max}(13)$	mmolg DW^{-1} day^{-1}	7.0601	19.9574
41	$v_{\max}(14)$	mmolg DW^{-1} day^{-1}	37.8124	40.2709
42	$v_{\max}(15)$	mmolg DW^{-1} day^{-1}	82.9691	61.5521
43	$v_{\max}(16)$	mmolg DW^{-1} day^{-1}	26.8950	12.2276
44	$v_{\max}(17)$	mmolg DW^{-1} day^{-1}	53.7900	28.5408
45	$v_{\max}(18)$	mmolg DW^{-1} day^{-1}	25.0320	62.1056
46	$v_{\max}(19)$	mmolg DW^{-1} day^{-1}	25.0207	117.3366
47	$v_{\max}(20)$	mmolg DW^{-1} day^{-1}	20.8500	83.4577

Table 5 continued

Parameter number	Symbols	Units	Initial parameters value $\boldsymbol{\theta}_0$	Pseudo-optimal initial set $\boldsymbol{\theta}^*$
48	$v_{max}(21)$	mmolg DW^{-1} day^{-1}	0.0030	0.0038
49	$v_{max}(22)$	mmolg DW^{-1} day^{-1}	0.0636	0.0290
50	$v_{max}(23)$	mmolg DW^{-1} day^{-1}	8.9713	8.4899
51	$v_{max}(24)$	mmolg DW^{-1} day^{-1}	0.8218	0.8327
52	$v_{max}(25)$	mmolg DW^{-1} day^{-1}	5.7975	1.3005
53	$v_{max}(26)$	mmolg DW^{-1} day^{-1}	3.4360	1.3605
54	$v_{max}(27)$	mmolg DW^{-1} day^{-1}	0.0306	0.0715
55	$v_{max}(28)$	mmolg DW^{-1} day^{-1}	0.7564	0.4617
56	$v_{max}(29)$	mmolg DW^{-1} day^{-1}	7.3666	5.0514
57	$v_{max}(30)$	mmolg DW^{-1} day^{-1}	0.0601	0.0860
58	$v_{max}(31)$	day^{-1}	0.5114	0.6003
60	$v_{max}(32)$	mmolg DW^{-1} day^{-1}	3×10^{-5}	5×10^{-6}
61	$v_{max}(33)$	mmolg DW^{-1} day^{-1}	1×10^{-5}	4×10^{-6}

[45, 46]. This matrix was scaled to ensure dimensional consistency using the following equation [11]:

$$s_{ij} = z_{ij} \frac{\Delta \theta_j}{SC_i} \qquad (9)$$

where z_{ij} was evaluated at $\boldsymbol{\theta}^*$, the point in the parameter space where the sensitivity analysis was carried out, $\Delta \theta_j$ is a scaling factor that reflects uncertainty in the initial guess for parameter θ_j, and SC_i is a scaling factor that reflects the uncertainty associated with the measurements. The sensitivity matrix was scaled using $\Delta \theta_j = 0.5$ according to Brun et al. [11], given that the values obtained in this work are the first ones reported for cell cultures of this specie. The value of SC_i was defined as the mean value for the output variables. The scaling of the sensitivity matrix is a central matter for the sensitivity analysis; therefore, in this work, the scaled sensitivity matrix was standardized, subtracting off the mean for each column and dividing it by the standard deviation [47].

The orthogonal method proposed by Yao et al. [18] was used in this work as the routine to determine identifiable parameters. This method sequentially applies orthogonal projections of the sensitivity vectors columns of the standardized sensitivity matrix to select one identifiable parameter at a time. The maximum number of parameters that can be identified was determined from the singularity of fisher information matrix (FIM), because this value indicates when the estimation problem becomes ill posed. The sensitivity matrix is related to the FIM using the following equation [44]:

$$\text{FIM} = S_{\boldsymbol{\theta}^*}^T Q S_{\boldsymbol{\theta}^*} \qquad (10)$$

where Q corresponds to the inverse measurement error covariance matrix and $S_{\boldsymbol{\theta}^*}$ is the standardized sensitivity matrix for the pseudo-optimal set of parameters obtained after optimization. This work assumes that the measurement of noise is uncorrelated and constant with the time; therefore, the covariance matrix results in an identity matrix and the FIM becomes the product of the transpose of sensitivity matrix itself [48].

Materials and methods

Cell suspensions

Cell suspensions were obtained from friable callus which were transferred to the shake flask with 80 ml of liquid SH medium. The cultures were maintained in an orbital shaker (IK KS501 digital) at 110 rpm and ambient temperature under natural photoperiod and subcultured every 12–15 days. Experiments were performed in liquid medium supplemented with sucrose [1].

Analytical methods

The samples were initially homogenized. Three milliliters of each sample were taken and filtered in vacuum for biomass determination using the dry weight method. The rest of the sample was centrifuged at 5000 rpm for 10 min in a centrifuge SIGMA 2–16 kPa at 25 °C. The supernatant was separated and used to determine extracellular nutrients. The rest of the sample was rinsed and homogenized three times. Then, this material was again centrifuged at 5000 rpm for 10 min, the supernatant was discarded, and the rest of the material was used for the cellular lysis. These samples were sonicated during 4 h at 37 °C. Then, a solution of NaOH 2 N was added and the mixture was heated to 100 °C for 20 min. The solution was cooled

down at ambient temperature and centrifuged at 5000 rpm. Finally, the pH of the supernatant was adjusted between 6.5 and 7.5 to determine the intracellular nutrients.

The extracellular sugars were determined by an HPLC (Agilent), coupled to refractive index detector using a coregel 87P column and water as mobile phase, the testing time was 16 min. The column operates at 80 °C and the RID (infrared) and detector operate at 55 °C. The intracellular glucose was determined using anthrone reagent according to the proposed method by De Bruyn et al. [49]. Nitrates were determined using a method based on salicylic acid [50], and phosphates were determined using the ascorbic acid method [51].

Results and discussion

Results of the final identifiability analysis are presented in Table 6. These results indicate that the subset with the most sensitive and linearly independent parameters corresponds to the subset of size 19. The remaining parameters will conform the subset of fixed parameters [θ_{Fixed}]. The re-optimization of each subset (from the least identifiable to the most identifiable) leads to a decrease in the error function reaching a better fit of the predicted values to experimental data, as can be seen in Table 6.

The confidence intervals for the identifiable parameters were obtained using the covariance matrix. FIM is the inverse of the parameter estimation error covariance matrix

COV and provides the Cramer–Rao lower bound on the parameter estimation errors [52] which can be used to assess the estimation uncertainty of θ_K^* [53] as presented in the following equation:

$$COV \geq FIM^{-1}(\theta_K^*.). \tag{11}$$

Then, approximate standard errors $\sigma(\theta_K^*)$ for the estimated parameters can be calculated as the square root of the diagonal elements of the inverse of FIM, see the following equation:

$$\sigma(\theta_K^*) = [\sqrt{cov_{11}}, \sqrt{cov_{22}}, \ldots, \sqrt{cov_{mm}}]. \tag{12}$$

In Table 7, the results of the optimal set of parameters $\left\{\tilde{\theta} = \theta_k^* \cup \theta_{Fixed}\right\}$ and the confidence intervals for identifiable parameters are reported. The values of the confidence intervals were obtained using the standard deviation calculated by Eq. (12). Most of the identifiable parameters have acceptable values of confidence intervals. However, parameters 22, 24, 49, and 59 have unacceptable confidence intervals, which could indicate that these parameters are insensitive towards the experiments performed. Therefore, it is recommended to apply strategies of model-based optimal experimental design as a future work for this culture.

The results of the model adjustment using the optimal parameters $\left[\tilde{\theta}\right]$ are presented in Fig. 2a and b). These results show a good fit for biomass (x), extracellular

Table 6 Subsets of identifiable parameters according to the orthogonal method

Size	Subsets of identifiable parameters θ_k																		DET	MSE$_Y$
2	49	55																	20.972	23.064
3	49	55	58																21.427	23.064
4	49	55	58	24															20.673	23.064
5	49	55	58	24	15														21.745	23.059
6	49	55	58	24	15	59													20.946	23.064
7	49	55	58	24	15	59	27												18.249	23.108
8	49	55	58	24	15	59	27	10											19.120	23.108
9	49	55	58	24	15	59	27	10	19										19.817	23.108
10	49	55	58	24	15	59	27	10	19	9									20.390	23.108
11	49	55	58	24	15	59	27	10	19	9	4								20.859	23.108
12	49	55	58	24	15	59	27	10	19	9	4	6							20.872	23.108
13	49	55	58	24	15	59	27	10	19	9	4	6	11						21.228	23.108
14	49	55	58	24	15	59	27	10	19	9	4	6	11	13					20.351	23.108
15	49	55	58	24	15	59	27	10	19	9	4	6	11	13	5				20.641	23.108
16	49	55	58	24	15	59	27	10	19	9	4	6	11	13	5	22			20.093	23.108
17	49	55	58	24	15	59	27	10	19	9	4	6	11	13	5	22	57		20.339	23.277
18	49	55	58	24	15	59	27	10	19	9	4	6	11	13	5	22	57	35	20.161	23.593
19	49	55	58	24	15	59	27	10	19	9	4	6	11	13	5	22	57	35	8	20.364	23.593

Numbers at each column correspond to the parameter's number given in Table 5

Table 7 Optimal parameters for plant cell cultures of *T. peruviana* and confidence intervals (±) for identifiable parameters

Number	Parameters	Parameters value subset θ_K^*	Parameters value subset θ_{Fixed}	Parameters value. Final set $\tilde{\theta}$. Confidence intervals
1	KmESUC		24.8394	24.8394
2	KmEGLUC		34.7882	34.7882
3	KmEFRUC		76.2353	76.2353
4	KmGLUC	0.8919		$0.8919 \pm 4.45 \times 10^{-3}$
5	KmG6P	0.5379		$0.5379 \pm 8.61 \times 10^{-3}$
6	KmR5P	0.9643		$0.9643 \pm 2.89 \times 10^{-3}$
7	KmF6P		0.2498	0.2498
8	KmG3P	0.2512		$0.2512 \pm 2.89 \times 10^{-2}$
9	KmPEP	0.4567		$0.4567 \pm 8.64 \times 10^{-3}$
10	KmPYR	0.9600		$0.9600 \pm 3.49 \times 10^{-3}$
11	KmACOA	0.6452		$0.6452 \pm 5.49 \times 10^{-3}$
12	KmOXO		0.8660	0.8660
13	KmOAA	0.1091		$0.1091 \pm 1.68 \times 10^{-2}$
14	KmENO$_3$		37.7649	37.7649
15	KmNO$_3$	0.5103		$0.5103 \pm 3.24 \times 10^{-3}$
16	KmNH$_4$		0.6995	0.6995
17	KmO$_2$		3.97×10^{-8}	4×10^{-8}
18	KmEPi		16.6949	16.6949
19	KmPi	0.9186		$0.9186 \pm 4.61 \times 10^{-3}$
20	KmSTA		0.0538	0.0538
21	KmOP		0.2321	0.2321
22	KmLIP	0.0074		$0.0074 \pm 1.39 \times 10^{-2}$
23	KmORA		0.0575	0.0575
24	KmAA	0.0017		$0.0017 \pm 6.27 \times 10^{-3}$
25	KmCO$_2$		0.0017	0.0017
26	KmPPi		0.0054	0.0054
27	KmSTH	0.0435		$0.0435 \pm 6.08 \times 10^{-3}$
59	KIENO$_3$	8.1297		$8.1297 \pm 6.96 \times 10^{-3}$
28	$v_{max}(1)$		15.1748	15.1748
29	$v_{max}(2)$		44.0409	44.0409
30	$v_{max}(3)$		67.8724	67.8724
31	$v_{max}(4)$		63.6234	63.6234
32	$v_{max}(5)$		8.8845	8.8845
33	$v_{max}(6)$		6.3287	6.3287
34	$v_{max}(7)$		3.0724	3.0724
35	$v_{max}(8)$	0.4345		$0.4345 \pm 7.78 \times 10^{-2}$
36	$v_{max}(9)$		0.0026	0.0026
37	$v_{max}(10)$		54.6006	54.6006
38	$v_{max}(11)$		1.39×10^{-5}	1.04×10^{-5}
39	$v_{max}(12)$		0.0089	0.0089
40	$v_{max}(13)$		19.9574	19.9574
41	$v_{max}(14)$		40.2709	40.2709
42	$v_{max}(15)$		61.5521	61.5521
43	$v_{max}(16)$		12.2276	12.2276
44	$v_{max}(17)$		28.5408	28.5408
45	$v_{max}(18)$		62.1056	62.1056
46	$v_{max}(19)$		117.3366	117.3366
47	$v_{max}(20)$		83.4577	83.4577

Table 7 continued

Number	Parameters	Parameters value subset θ_K^*	Parameters value subset θ_{Fixed}	Parameters value. Final set $\tilde{\theta}$. Confidence intervals
48	$v_{max}(21)$		0.0038	0.0038
49	$v_{max}(22)$	3.9×10^{-6}		$3.9 \times 10^{-6} \pm 1.44 \times 10^{-4}$
50	$v_{max}(23)$		8.4899	8.4899
51	$v_{max}(24)$		0.8327	0.8327
52	$v_{max}(25)$		1.3005	1.3005
53	$v_{max}(26)$		1.3605	1.3605
54	$v_{max}(27)$		0.0715	0.0715
55	$v_{max}(28)$	0.9709		$0.9709 \pm 1.07 \times 10^{-3}$
56	$v_{max}(29)$		5.0514	5.0514
57	$v_{max}(30)$	0.0290		0.0290 ± 0.32
58	$v_{max}(31)$	0.4566		$0.4566 \pm 7.97 \times 10^{-4}$
60	$v_{max}(32)$		3×10^{-5}	5×10^{-6}
61	$v_{max}(33)$		1×10^{-5}	4×10^{-6}

The confidence intervals are based on the 95% significance level

sucrose (ESUC), intracellular glucose (GLU), and phosphates (Pi). In addition, the model presents a good prediction of the extracellular hydrolysis of sucrose (ESUC) into extracellular glucose (EGLUC) and fructose (EFRUC). However, to get a better fit of nitrates, it is necessary to perform additional studies to determine the effects of accumulation of these nutrients in the plant cell cultures of *T. peruviana*. The intracellular components reached the steady state by the 16th day approximately. As expected, nutrients as G6P, R5P, PEP, PYR, ACOA, OXO, and OAA increased their concentrations approximately until the 5th day corresponding to lag phase. This behavior is normal given that the cells adapt during this phase with low demands of the nutrients. Then, these nutrients presented a notable decrease in the slope approximately at the 10th day, which corresponds to the start of the exponential phase. This phase implies high requirements of nutrients. Finally, around the 16th day, these nutrients reached steady state close to the time corresponding to the stationary phase. For F6P, an increase was observed until the 10th day where a steady state was reached. G3P then begins to increase from that day. The biomass precursors, STH, OP, ORA, LIP, and AA, follow a similar trend to the cell growth, they are increasing their concentration and reaching the steady state close to the 16th day. This corresponds to the stationary phase for cell growth. The upper and lower bounds in the extracellular components are quite similar to the reported by Cloutier et al. [34]. In the case of intracellular components, similar bounds were found for PEP, PYR, ACOA, and OXO. The reactions for metabolite production presented by Cloutier et al. [34] could generate the differences in the bounds of the other intracellular components with respect to this work, since this research only includes the reactions for biomass production. In Fig. 2c, the results of the model predictions using validation data (i.e. a complete different set from the two used above for identifying the parameters) are presented. Validation results indicate that the model presents good predictive capability in the range of the initial conditions used for the model construction.

Although the model proposed in this study for plant cell cultures of *T. peruviana* is based on similar mechanistic models as the presented in Cloutier et al. [34] for cultures of *C. roseus* hairy root, and Cloutier et al. [35] for plant cell cultures of *E. californica*, each cellular species present a different set of parameter values. Such differences in the parameter values reflect differences in the cellular physiology among the plant cell cultures studied. For instance, in this work, the value of affinity constant for ACOA correspond to 0.6452 mmolg DW^{-1}, this value is higher than the reported to *C. roseus* hairy root corresponding to 0.0125 mmolg $DW^{-1,}$ and the reported to *E. californica* corresponding to 0.0024 mmolg DW^{-1}. The obtained value in the case of *T. peruviana* indicates its low affinity for this substrate in comparison with the others plant cell cultures analyzed. In the case of biomass precursors, it is possible to conclude that the plant cell cultures of *T. peruviana* present a high tendency to accumulate nutrients, given its low value of the affinity constant to *STA* corresponding to 0.0538 mmolg DW^{-11}, which is lower than the reported to *C. roseus* hairy root which corresponds to 1 mmolg DW^{-1} and the reported to *E. californica* corresponds to 0.94 mmolg DW^{-1}.

Fluxes distribution in plant cell cultures of *T. peruviana*

Figure 3 shows the fluxes distribution for plant cell cultures
of *T. peruviana* for the stationary phase, between the 10th
day, when the exponential phase is ending, and 16th day
when the stationary phase is ending (before cells dead).
The fluxes were evaluated using the results of the kinetics
corresponding to an initial inoculum concentration of
2.41 g/L, and an initial sucrose concentration of 22.64 g/L.

It can be seen that the flux of the reaction representing
the hydrolysis of sucrose into glucose and fructose $v(1)$
decreases in 96.46% between the 10th day and the 16th
day. This decrease suggests that the hydrolysis of sucrose
for this plant cell culture is mainly performed at extracel-
lular level. The change in flux $v(2)$ (reaction in which
glucose becomes intracellular glucose) shows a decrease of
95.58% between the 10th day and the 16th day. This value
is higher than the change experienced in flux $v(3)$ (reaction
in which fructose becomes intracellular glucose), for which
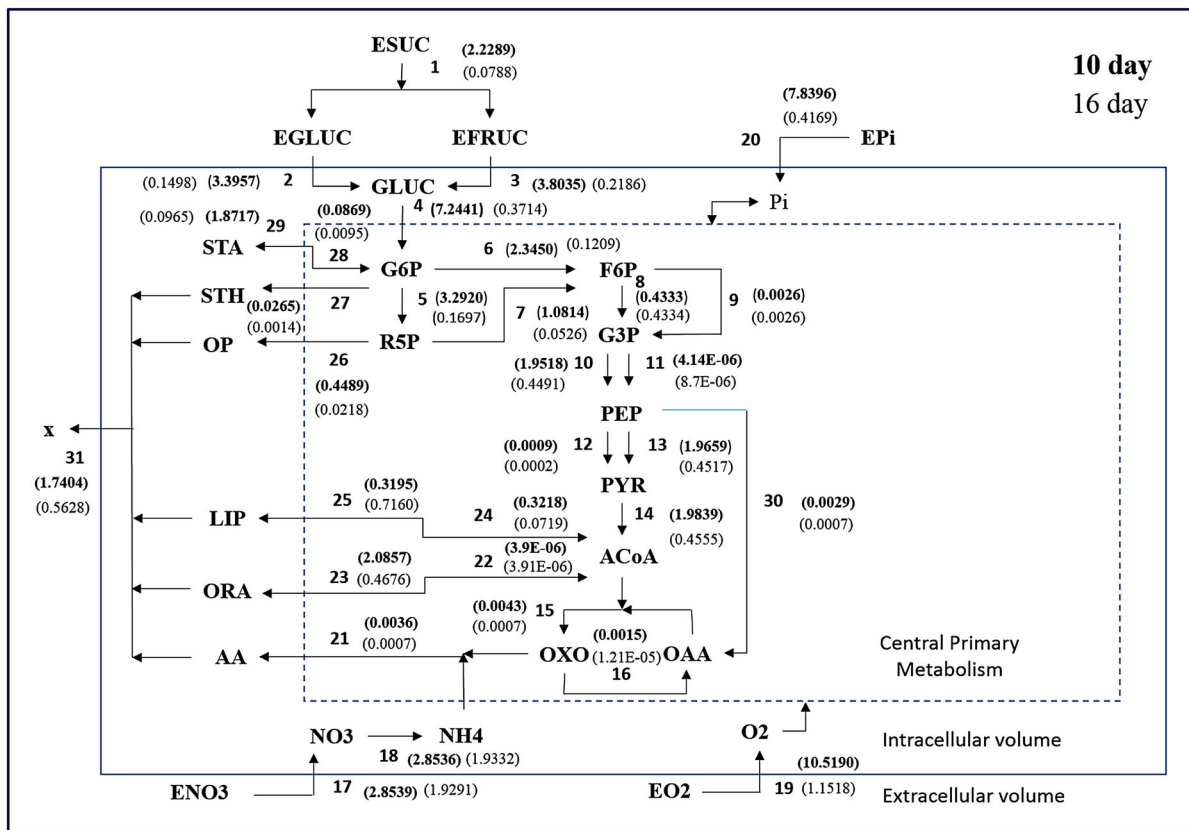
Fig. 3 Flux distribution for plant cell cultures of *Thevetia peruviana*. Values in *bold* correspond to the 10th day of culture

a decrease of 94.33% was observed. This behavior indicates that the cells consume preferably glucose as source of energy. However, the closeness of the values indicates that the cell is carrying out a parallel uptake of both nutrients, but with preference on glucose. This differentiated uptake of sugars was reported by Krook et al. [54] for cell suspension of *Daucus Carota,* and could be due to the fact that the glucose is a better substrate in cellular respiration processes than the fructose.

It is observed that the variation in the flux $v(20)$ (extracellular phosphates) is higher than the flux $v(17)$ (extracellular nitrates) with changes the 96.68 and of 32.40%, respectively. This indicates a high demand of phosphates and an initial accumulation of nitrates, which is in agreement with the experimental results obtained in this work.

The main route for the glycolysis pathway is determined through the fluxes: $v(8)$, $v(10)$, $v(11)$, $v(13)$, and $v(14)$. Although in the formation of Glyceraldehido-3-phosphate from Fructose-6-phosphate, the fluxes $v(8)$ and $v(9)$ practically reach the steady state, the change on flux $v(8)$ is slightly higher than the flux $v(9)$. The glyceraldehido-3-phosphate is transformed in phosphoenolpyruvate through the flux $v(10)$ with a change of 76.99%, which is higher than the flux $v(11)$ with a change of 52.41%. In addition, finally, the transformation of phosphoenolpyruvate to pyruvate is preferably

carried out through of the flux $v(12)$ with a change of the 77.77% higher than the flux $v(13)$ with a variation of 77.02%.

Analyzing the biomass precursors, it is observed that the fluxes $v(26)$ (organic phosphates), $v(27)$ (structural hexoses), $v(21)$ (amino acids), $v(23)$ (organic acids), and the $v(25)$ (lipids) experienced variations of 95.14, 94.71, 80.55, 77.58, and 55.37%, respectively. The high demand of organic phosphates as precursors of biomass formation could explain the significant changes in the flux of phosphates $v(20)$. The high demand of amino acids is understandable given its important role in protein formation. Between the 10th and the 16th day, the demand of lipids is low in comparison with the other precursors, since the cells could preferably accumulate them, as can be observed in its flux value.

The changes of the flux values found for the flux $v(29)$ corresponding to the reserves of starch were 94.84%, indicating the importance of these reserves for the maintenance of the cells at the end of the growth.

Conclusions

In this work, a new mechanistic model for plant cell cultures of *T. peruviana* was developed. The identifiability analysis indicated that only 19 parameters of the model are

identifiable parameters, suggesting high correlations among parameters effects for this type of models. The analysis of fluxes distributions indicates the behavior and tendencies in the nutrients uptake for this culture. This work is the base for the development of future works in the determination of routes for metabolite production from plant cell cultures of *T. peruviana*. The information about parameters value for the proposed mechanistic model contributes to the pool of available parameters for the modelling of plant cell cultures. Nonetheless, future work in the application and development of methodologies for identification and strategies for model-based optimal experimental design are required to improve the predictive capabilities of plant cell culture models.

Compliance with ethical standards

Conflict of interest The authors declare that they have no competing interest

References

1. Arias M, Angarita MJ, Restrepo JM et al (2009) Elicitation with methyl-jasmonate stimulates peruvoside production in cell suspension cultures of Thevetia *peruviana*. Vitr Cell Dev Biol Plant 46:233–238. doi:10.1007/s11627-009-9249-z

2. Siwach P, Grover K, Gill AR (2011) The influence of plant growth regulators, explant nature and sucrose concentration on in vitro callus growth of *Thevetia peruviana* schum. Asian J Biotechnol 3:280–292

3. Kohls S, Scholz-Böttcher BM, Teske J et al (2012) Cardiac glycosides from Yellow Oleander (*Thevetia peruviana*) seeds. Phytochemistry 75:114–127. doi:10.1016/j.phytochem.2011.11.019

4. Tian D-M, Cheng H-Y, Jiang M-M et al (2015) Cardiac Glycosides from the Seeds of *Thevetia peruviana*. J Nat Prod 79:38–50. doi:10.1021/acs.jnatprod.5b00611

5. Amaringo FV, Hormaza A, Arias M (2011) Thevetin B: glicósido cardiotónico predominante en *Thevetia peruviana*. Sci Tech 298–303

6. Rincón-pérez J, Rodríguez-hernández L, Ruíz-valdiviezo VM et al (2016) Fatty acids profile, phenolic compounds and antioxidant capacity in elicited callus of *Thevetia peruviana* (Pers.) K. Schum. J Oleo Sci 318:311–318

7. Cloutier M, Bouchard-Marchand É, Perrier M, Jolicoeur M (2008) A Predictive nutritional model for plant cells and hairy roots. Biotechnol Bioeng 99:189–200. doi:10.1002/bit

8. Leduc M, Tikhomiroff C, Cloutier M et al (2006) Development of a kinetic metabolic model: application to *Catharanthus roseus*

9. hairy root. Bioprocess Biosyst Eng 28:295–313. doi:10.1007/s00449-005-0034-z

9. Alberton KPF, Alberton AL, Di Maggio JA et al (2015) Simultaneous parameters identifiability and estimation of an *E. coli* metabolic network model. Biomed Res Int 2015:1–21. doi:10.1155/2015/454765

10. Balsa-Canto E, Alonso AA, Banga JR (2010) An iterative identification procedure for dynamic modeling of biochemical networks. BMC Syst Biol 4:11. doi:10.1186/1752-0509-4-11

11. Brun R, Reichert P, Ku HR (2001) Practical identi ability analysis of large environmental simulation models. Water Resour Res 37:1015–1030

12. Degenring D, Froemel C, Dikta G, Takors R (2004) Sensitivity analysis for the reduction of complex metabolism models. J Process Control 14:729–745. doi:10.1016/j.jprocont.2003.12.008

13. Jiménez-Hornero JE, Santos-Dueñas IM, García-García I (2009) Optimization of biotechnological processes. The acetic acid fermentation. Part II: practical identifiability analysis and parameter estimation. Biochem Eng J 45:7–21. doi:10.1016/j.bej.2009.01.010

14. Kravaris C, Hahn J, Chu Y (2013) Advances and selected recent developments in state and parameter estimation. Comput Chem Eng 51:111–123. doi:10.1016/j.compchemeng.2012.06.001

15. López DC, Barz T, Peñuela M et al (2013) Model-based identifiable parameter determination applied to a simultaneous saccharification and fermentation process model for bio-ethanol production. Biotechnol Prog 29:1064–1082. doi:10.1002/btpr.1753

16. Mailier J, Delmotte A, Cloutier M et al (2011) Parametric sensitivity analysis and reduction of a detailed nutritional model of plant cell cultures. Biotechnol Bioeng 108:1108–1118. doi:10.1002/bit.23030

17. Weijers SR, Vanrolleghem PA (1997) A procedure for selecting best identifiable parameters in calibrating activated sludge model No. 1 to full-scale plant data. Water Sci Technol 36:69–79. doi:10.1016/S0273-1223(97)00463-0

18. Yao KZ, Shaw BM, Kou B et al (2003) Modeling ethylene/butene copolymerization with multi-site catalysts: parameter estimability and experimental design. Polym React Eng 11:563–588. doi:10.1081/PRE-120024426

19. Almquist J, Cvijovic M, Hatzimanikatis V et al (2014) Kinetic models in industrial biotechnology: improving cell factory performance. Metab Eng 24:38–60. doi:10.1016/j.ymben.2014.03.007

20. Bramble JL, Graves DJ, Brodelius P (1991) Calcium and phosphate effects on growth and alkaloid production in *Coffea arabica*: experimental results and mathematical model. Biotechnol Bioeng 37:859–868. doi:10.1002/bit.260370910

21. Hooker BS, Lee JM (1992) Application of a new structured model to tabacco cell cultures. Biotechnology 39:765–774

22. van Gulik WM, ten Hoopen HJG, Heijnen JJ (1992) Kinetics and stoichiometry of growth of plant cell cultures of *Catharanthus roseus* and *Nicotiana tabacum* in batch and continuous fermentors. Biotechnol Bioeng 40:863–874. doi:10.1002/bit.260400802

23. Takeda T, Takeuchi T, Seki M et al (1998) Kinetic analysis of cell growth and vitamin E production in plant cell culture of *Carthamus tinctorius* using a structured model. Biochem Eng J 1:233–242

24. Choi J-W, Kim Y-K, Lee WH et al (1999) Kinetic model of cell growth and secondary metabolite synthesis in plant cell culture of *Thalictrum rugosum*. Biotechnol Bioprocess Eng 4:129–137

25. Choi J-W, Kim Y-K, Park H-K et al (1999) Kinetic model for biotransformation of digitoxin in plant cell suspension culture of *Digitalis lanata*. Biotechnol Bioprocess Eng 4:281–286

26. Schlatmann JE, Ten Hoopen HJG, Heijnen JJ (1999) A simple structured model for maintenance, biomass formation, and

ajmalicine production by nondividing *Catharanthus roseus* cells. Biotechnol Bioeng 66:147–157. doi:10.1002/(SICI)1097-0290(1999)66:3<147:AID-BIT2>3.0.CO;2-N

27. Pires Cabral PMN, Lima Costa ME, Cabral JMS (2000) A structured growth model for *Cynara cardunculus* cell suspension. Bioprocess Eng 23:199–203. doi:10.1007/s004499900151

28. Zhang J, Su WW (2002) Estimation of intracellular phosphate content in plant cell cultures using an extended Kalman filter. J Biosci Bioeng 94:8–14. doi:10.1263/jbb.94.8

29. Li C, Yuan Y-J, Wu J-C, Hu Z-D (2003) A structured kinetic model for suspension cultures of *Taxus chinensis* var. mairei induced by an oligosaccharide from *Fusarium oxysporum*. Biotechnol Lett 25:1335–1343. doi:10.1023/A:1024980420790

30. Villadsen J, Nielsen J, Lidén G (2011) Bioreaction Engineering principles, Third

31. Bellgardt K-H (2000) Bioprocess Models. In: Schügerl K, Bellgardt K-H (eds) Bioreact. Eng. Model. Control, 1st ed. Springer-Verlag Berlin Heidelberg, pp 44–105

32. Wiechert W, Noack S (2011) Mechanistic pathway modeling for industrial biotechnology: challenging but worthwhile. Curr Opin Biotechnol 22:604–610. doi:10.1016/j.copbio.2011.01.001

33. Alberton KPF, Alberton AL, Di Maggio JA et al (2013) Accelerating the parameters identifiability procedure: set by set selection. Comput Chem Eng 55:181–197. doi:10.1016/j.compchemeng.2013.04.014

34. Cloutier M, Perrier M, Jolicoeur M (2007) Dynamic flux cartography of hairy roots primary metabolism. Phytochemistry 68:2393–2404. doi:10.1016/j.phytochem.2007.04.028

35. Cloutier M, Chen J, Tatge F et al (2009) Kinetic metabolic modelling for the control of plant cells cytoplasmic phosphate. J Theor Biol 259:118–131. doi:10.1016/j.jtbi.2009.02.022

36. Cloutier M, Chen J, De Dobbeleer C et al (2009) A systems approach to plant bioprocess optimization. Plant Biotechnol J 7:939–951. doi:10.1111/j.1467-7652.2009.00455.x

37. Prakash G, Srivastava AK (2006) Modeling of azadirachtin production by *Azadirachta indica* and its use for feed forward optimization studies. Biochem Eng J 29:62–68. doi:10.1016/j.bej.2005.02.027

38. Omar R, Abdullah MA, Hasan MA et al (2006) Kinects and modelling of cell growth and substrate uptake in *Centella asiatica* cell culture. Biotechnol Bioprocess Eng 11:223–229

39. Yang SM, Shao DG, Luo YJ (2005) A novel evolution strategy for multiobjective optimization problem. Appl Math Comput 170:850–873. doi:10.1016/j.amc.2004.12.025

40. Shibasaki N, Obika R, Yonemoto T, Tadaki T (1995) Kinetic-analysis for effect of initial substrate concentration on growth and secondary metabolite production in cultures of *Nicotiana-tabacum*. J Chem Technol Biotechnol 63:201–208

41. Westgate PJ, Emery AH, Hasegawa PM, Heinstein PF (1991) Microbiology biotechnology growth of *Cephalotaxus harrin* ltonia plant-cell cultures. Appl Microbiol Biotechnol 34:798–803

42. Li C, Yuan Y, Wu J, Hu Z (2003) A structured kinetic model for suspension cultures of Taxus chinensis var. mairei induced by an oligosaccharide from *Fusarium oxysporum*. Biotechnol Lett 25:1335–1343

43. Sun J, Zhang C, Zhang X et al (2012) Extracellular ATP signaling and homeostasis in plant cells. Plant Signal Behav 7:566–569. doi:10.4161/psb.19857

44. McLean KAP, McAuley KB (2012) Mathematical modelling of chemical processes-obtaining the best model predictions and parameter estimates using identifiability and estimability procedures. Can J Chem Eng 90:351–366. doi:10.1002/cjce.20660

45. Ataíde F, Hitzmann B (2009) When is optimal experimental design advantageous for the analysis of Michaelis–Menten kinetics? Chemom Intell Lab Syst 99:9–18. doi:10.1016/j.chemolab.2009.07.005

46. Yue H, Brown M, Knowles J et al (2006) Insights into the behaviour of systems biology models from dynamic sensitivity and identifiability analysis: a case study of an NF-kappaB signalling pathway. Mol BioSyst 2:640–649. doi:10.1039/b609442b

47. Bendtsen AB, Glarborg P, Dam-Johansen K (2001) Visualization methods in analysis of detailed chemical kinetics modelling. Comput Chem 25:161–170. doi:10.1016/S0097-8485(00)00077-2

48. Chu Y, Hahn J (2009) Parameter set selection via clustering of parameters into pairwise indistinguishable groups of parameters. Ind Eng Chem Res 48:6000–6009. doi:10.1021/ie800432s

49. De Bruyn JW, Van Keulen HA, Ferguson JHA (1968) Rapid method for the simultaneous determination of glucose and fructose using anthrone reagent. JSci Fd Agric 19:597–601

50. Cataldo DA, Maroon M, Schrader LE, Youngs VL (1975) Rapid colorimetric determination of nitrate in plant tissue by nitration of salicylic acid. Commun Soil Sci Plant Anal 6:71–80. doi:10.1080/00103627509366547

51. Eaton A, Clesceri L, Greenberg A, Franson M (1998) Standard methods for the examination of water and wastewater. part 4000 inorganic nonmetallic constituents. Stand. Methods Exam. Water Wastewater

52. Petersen B, Gernaey K, Vanrolleghem PA (2001) Practical identifiability of model parameters by combined respirometric-titrimetric measurements. Water Sci Technol 43:347–355

53. Gadkar KG, Gunawan R, Doyle FJ (2005) Iterative approach to model identification of biological networks. BMC Bioinformatics 6:155. doi:10.1186/1471-2105-6-155

54. Krook J, Vreugdenhil D, Van Der Plas LHW (2000) Uptake and phosphorylation of glucose and fructose in *Daucus carota* cell suspensions are differently regulated. Plant Physiol Biochem 38:603–612. doi:10.1016/S0981-9428(00)00776-2